Monitoring Satellites by Comparing Infrared Observations to a Multi-Component Thermal Model

Stephen Catsamas[1], Sarah Caddy[1], Michele Trenti[1]
[1]*School of Physics, The University of Melbourne, Parkville, 3010, Australia*

ABSTRACT

All resident space objects (RSOs) emit hard to mask thermal infrared radiation which is linked by their shape, composition and operational status. Infrared imaging at multiple wavelengths can be used to sample this radiation (or infrared spectrum) from spatially unresolved remote observations of RSOs all the way out to geostationary orbit and beyond, opening the opportunity to gain insight on the objects. In this work, to understand the activity and operations of a satellite from these observations, we compare them to multi-component thermal models, improving upon the current state of the art approach of measuring a single (average) temperature. We derive analytic thermal and infrared spectral models for satellites and present how the spectrum changes with variables such as observation perspective and internal power usage. We motivate and introduce a two-component satellite model where both components have their own temperature and emissive properties and correspond to a component of the satellite such as a chassis or solar arrays. First, we demonstrate that non-linear least squares regression can be used to fit this two-component model from idealized unresolved thermal infrared space telescope observations. Furthermore, assuming observations with a small (≈ 0.5 m aperture) space telescope - similar to the NASA WISE mission - uncertainties of a few Kelvin can be achieved on both model components. Interestingly, a temperature difference well above 10 K is expected for a chassis and solar arrays of an idle spacecraft due to the typical radiative geometry. Hence, our modeling has the potential to measure the temperature of both these components individually through IR observations. We also discuss the implications our results hold for monitoring solar panel to chassis power flows in operational spacecraft. As a first step towards assessing feasibility and cost of a space-based IR telescope for space domain awareness, we present preliminary constraints on the wavelength range to consider for the observations. This range is constrained at one end from increases in cost and complexity for longer wavelength observations, as significant telescope baffle cooling is required to prevent excessive instrumental and foreground noise. On the other end, solar radiation begins to dominate the spectrum at shorter wavelengths. Qualitatively, observing in the range 3-10 micron represents a good compromise between performance and current technological capabilities. Overall, our results show that an infrared space telescope holds clear prospects for RSO classification and categorization, and thus would be a valuable space domain awareness asset.

1. INTRODUCTION

The number of tracked objects in Earth's orbit currently sits at near 45 000, a doubling over the count since last decade. This rapid growth is shown in fig. 1. Crucially, over this same time period, the number of resident space objects (RSOs) of unknown classification has markedly increased to now comprise 22 % of all objects. Therefore, new capabilities to characterize and monitor RSO are needed.

Ground-based radar and optical facilities form the backbone of current space domain awareness facilities [15]. While these system provide comprehensive cataloging of RSO [9], ground-based systems have high latency due to the need for the RSO to be above the horizon. Optical systems have further weather and illumination condition requirements which restrict observations and radar observations may be inhibited by stealth satellite designs [16].

To provide new capabilities more suited towards RSO characterization and monitoring, space-based systems have been considered [6, 8, 17, 1, 3, 2, 10]. Among these are Non-Earth Imaging satellites, which provide resolved imagery of RSO in Low Earth Orbit (LEO) [2, 10]. Extension of this concept to Geostationary Earth Orbit (GEO) targets is however challenging as telescope apertures in excess of those of the Hubble Space Telescope - i.e. several meters in diameter - would be required to overcome the diffraction limit for GEO RSOs smaller than ≈ 10 m observed from LEO.

Copyright © 2025 Advanced Maui Optical and Space Surveillance Technologies Conference (AMOS) – www.amostech.com

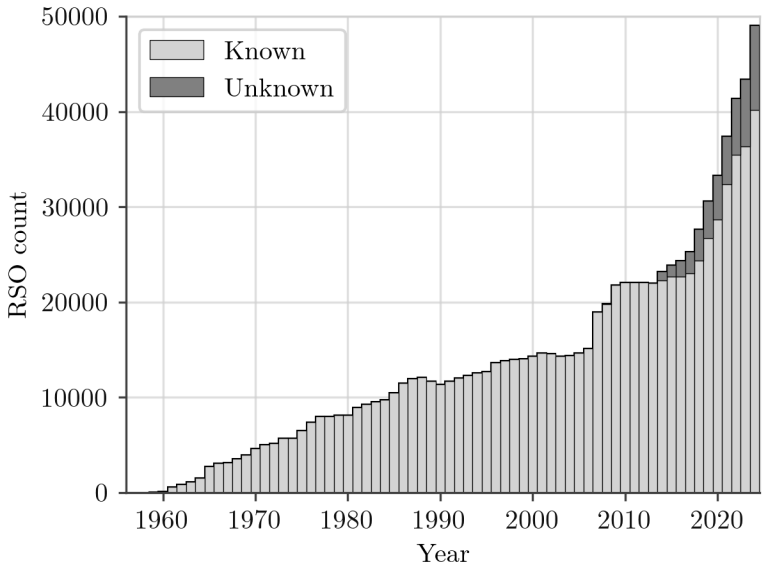

Fig. 1: In-orbit tracked RSO count by year. The rate of RSO count increase underwent a step change around 2010 and has increased at an average rate of 2000/year since this date (c.f. 400/year for the first 50 years of spaceflight). Alongside this new rapid growth in RSO count has emerged the presence of a large number of RSOs of unknown classification. Together these trends motivate the need for novel RSO characterization and classification capabilities. Data sourced from ESA DISCOS (Database and Information System Characterising Objects in Space; 2024).

Infrared observations of RSO have been a recent frontier of SDA research. Interest in infrared observation is motivated by relaxed RSO illumination requirements (the light flux is from thermal emission rather than reflection of sunlight) and rich spectrum-encoded information (thus not requiring spatially resolved observations). This includes information about a spacecraft's activities and operations [11]. An observation of an RSO in the thermal infrared is provided in fig. 2 which displays images of Echostar 4 (NORAD: 25331) serendipitously acquired by NASA's Wide-field Infrared Survey Explorer (WISE) in each of it's four bands ranging from 3.4 µm to 22 µm. The RSO forms a streak in this image as it moves across the field of view during the exposure.

Of SDA studies focusing on the infrared, several have explored establishing relationships between color distributions and photometric brightness and satellite geometries (box-wing, cylindrical), RSO size, and material properties [4, 7, 14, 13]. Other studies have explored modeling the RSO as a single temperature body emitting thermal radiation to discriminate between payloads and rocket bodies [12] or spacecraft activities [18]. While these studies lay promising ground-work for infrared SDA, ascribing a single temperature to an RSO neglects the independent thermal behavior of RSO components, particular the solar panels and chassis of box-wing type satellites.

In this work we first discuss the principles of thermal infrared RSO characterization. We then motivate a two-component spectral model suited to monitoring box-wing type satellites. For this model we determine to what uncertainty parameters such as component temperatures can be inferred and the how these results depend on the range of satellite temperatures and maximum infrared observation wavelength. We discuss the implication our results hold for monitoring satellite power flows and maneuver detection, and the implications our observation wavelength range investigation results hold for design of a IR space telescope for space domain awareness.

2. PRINCIPLES OF THERMAL INFRARED OBSERVATIONS

For an RSO, or, more accurately, RSO component, to maintain a steady state temperature, stored internal power use and heat flows into the RSO component must be balanced by heat flows out of the RSO component. In the vacuum of space, dissipation of heat via convection is not possible and thus heat is exchanged with the ambient via radiation. Heat flow into the RSO component is dominated by solar radiation which provides an irradiance of $I_\odot = 1360\,\mathrm{W/m^2}$; in spacecraft, use of stored internal power to perform operations may also generates substantial heat; Earthshine (light

Copyright © 2025 Advanced Maui Optical and Space Surveillance Technologies Conference (AMOS) – www.amostech.com

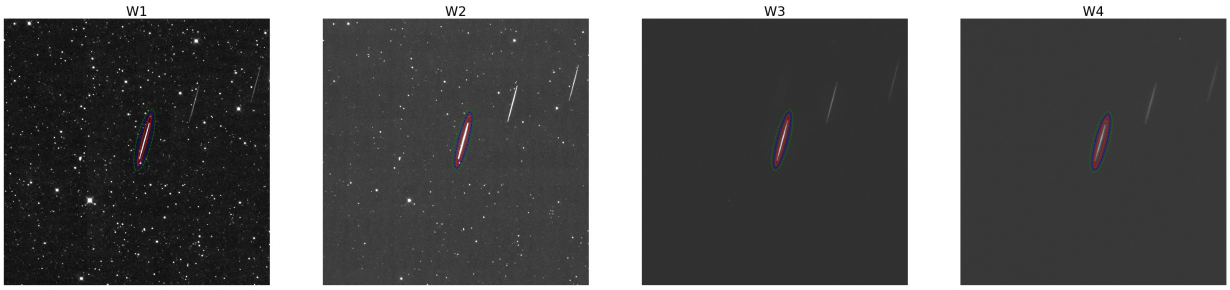

Fig. 2: Echostar 4 (NORAD: 25331) imaged by the WISE space telescope on 2010 February 13 at 11:16 UTC. The four photometric bands have wavelengths: W1 = 3.4 µm, W2 = 4.6 µm, W3 = 12 µm, and W4 = 22 µm. Exposure times are 7.7 s in W1 and W2 and 8.8 s in W3 and W4.

	Spherical Chassis	**Rectangular Planar Solar Array**
Dimensions	$r = 1\,\mathrm{m}$	$l = w = \sqrt{\pi}\mathrm{m}$
Surface Area, A	$4\pi\mathrm{m}^2$	$2\pi\mathrm{m}^2$
Illuminated Area, A_{ill}	$\pi\mathrm{m}^2$	$\pi\mathrm{m}^2$
Absorptivity, α	0.3	0.8
Emissivity, ε	0.6	0.8
Temperature, T_{RC}	234 K	324 K
Temperature Power Dependence, $\frac{\mathrm{d}T_{RC}}{\mathrm{d}P_{\mathrm{int}}}$	46 K/kW	26 K/kW

Table 1: Illustrative steady state temperatures for a spherical chassis RSO component and a sun-facing planar solar array RSO component. Absorptivity and emissivity values for a Kapton insulated chassis and solar cells have been assumed [5].

scattered and emitted from the surface of the Earth) provides lesser contribution, assumed to be negligible in this work. This heat is rejected by the RSO component emitting it's own radiation of equal power.

To first order the RSO component radiates as a greybody radiator. For a greybody the radiative power is given by:

$$P = \varepsilon A \sigma_{\mathrm{SB}} T_{\mathrm{RC}}^4 \tag{1}$$

where T_{RC} is the temperature of the RSO component, A it's surface area, $\sigma_{\mathrm{SB}} = 5.67 \times 10^{-8}\,\mathrm{Wm}^{-2}\mathrm{K}^{-4}$ the Stefan-Boltzmann constant, and $0 \leq \varepsilon \leq 1$ is the emissivity which is an empirically determined surface property which specifies how effectively the surface radiates. Heat balance can therefore be expressed as the equation:

$$P_{\mathrm{int}} + \alpha A_{\mathrm{ill}} I_{\odot} = \varepsilon A \sigma_{\mathrm{SB}} T_{\mathrm{RC}}^4, \tag{2}$$

where P_{int} is the net internal power usage, $0 \leq \alpha \leq 1$ is the solar absorptivity of the RSO component's surface and A_{ill} it's illuminated area. For a broad range of surface properties and geometries, temperatures of about 250 K to 350 K are expected. To illustrate this, table 1 outlines the steady state temperature for RSO components of a spherical chassis and sun-facing planar solar arrays. Note that the spherical chassis has a lower steady state temperature as both a) while it's illuminated area is equal to that of the planar solar arrays, it has twice the surface area to radiate from and b) Kapton insulation has a larger ε/α ratio is relatively less effective at absorbing solar radiation than the solar cells. This large spread in steady state temperatures highlights the limitations of assigning a single temperature to unresolved observation; RSO which consist of multiple components such as box-wing type satellites, will have multiple steady state temperatures. Table 1 also calculates the dependence of steady state temperatures on internal power usage using eq. (2). For the ≈ 1 m radius components considered here, these temperatures depend on the order of 10s of Kelvin per kilowatt of net internal power usage.

In addition the total radiated power of thermal emissions, the spectrum of this radiation is well-modeled by Planck's

Copyright © 2025 Advanced Maui Optical and Space Surveillance Technologies Conference (AMOS) – www.amostech.com

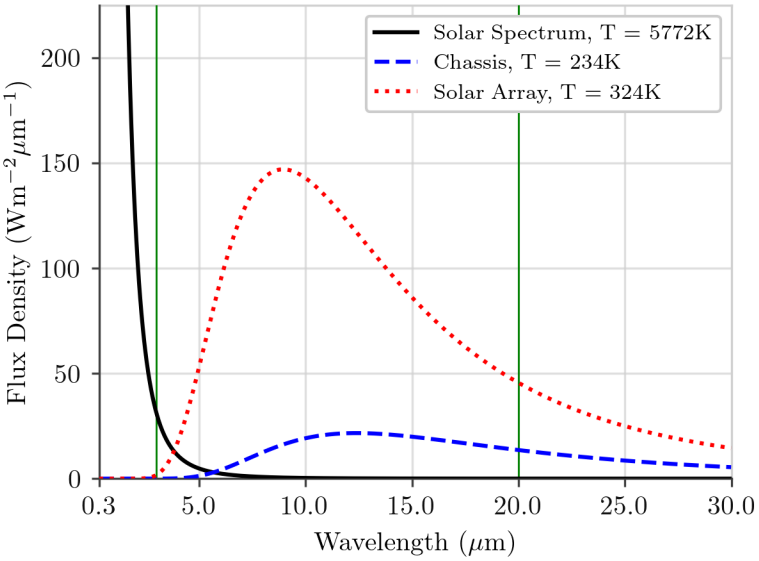

Fig. 3: Spectral irradiance for an RSO component at $T = 234\,\mathrm{K}$ (dashed blue) and $T = 324\,\mathrm{K}$ (dotted red) and typical reflected solar spectrum (solid black). The RSO component spectrum peaks between $\approx 3\,\mu\mathrm{m}$ to $20\,\mu\mathrm{m}$ (green vertical lines) in what is termed the thermal infrared. Minimal overlap exists between the reflected solar spectrum and RSO component emission.

law:

$$I(\lambda, \varepsilon, A, T_{\mathrm{RC}}) = \varepsilon A B(\lambda, T_{\mathrm{RC}}) \tag{3}$$

$$B(\lambda, T_{\mathrm{RC}}) \propto \lambda^{-5} \left(\exp(hc/\lambda k_B T_{\mathrm{RC}}) - 1\right)^{-1}, \tag{4}$$

Where h is Planck's constant, c is the speed of light, k_B is Boltzmann's constant and λ is the wavelength of the emitted radiation. This spectrum is presented in fig. 3 for the spherical chassis and planar solar arrays RSO components. The majority of this emission occurs in the infrared between $\approx 3\,\mu\mathrm{m}$ to $20\,\mu\mathrm{m}$. Over the majority of this range, the reflected solar spectrum is much less intense than the RSO component's own infrared emissions and can be neglected leaving the RSO component emissions as the only significant contributor. Importantly, relatively few parameters $A, \varepsilon, T_{\mathrm{RC}}$ are needed to model the component's spectrum and of these the temperature uniquely determines the width and position of the spectrum's peak. Due to this, for isolated components, it is possible to infer the component temperature of the RSO by sampling the spectrum at a few wavelengths and without requirements for additional information about the RSO.

To conclude, we emphasize the following key points

1. infrared emission is required to maintain steady RSO component temperatures and thus, unlike optical or radar signatures, masking or minimizing this thermal infrared emission is not feasible,
2. RSO operations which source or sink significant power, such as battery charging, data transmission, or electric thruster use, change the temperature of RSO components and thus it's infrared emission spectrum,
3. as the RSO component's spectrum in the thermal infrared is governed by Planck's law, the emission temperature can be inferred from observations of the spectrum.
4. this temperature can encode rich information about an RSO's operations and activities.

3. A TWO-COMPONENT SATELLITE MODEL

In order to infer information about the on-board operations of a more complex RSO like a satellite, a more detailed two-component thermal model is required to capture differences in temperature between satellite components. In the

Copyright © 2025 Advanced Maui Optical and Space Surveillance Technologies Conference (AMOS) – www.amostech.com

preceding introduction to thermal infrared RSO observation, only the spectrum consisting of emission from a single RSO component is considered. While this may be an appropriate model for more monolithic and smaller RSO such as space debris or natural rocks, more structured RSO such as satellites and rocket bodies may not achieve a single steady state temperature. For example, a box-wing type satellite consists principally of a central chassis and extended solar arrays. These components are relatively thermally isolated and thus are expected to obtain different steady state temperatures, similar to what they would obtain in isolation. Using the example components presented in table 1 gives a temperature of 234 K for the chassis and 324 K for the solar arrays - a 90 K difference. For unresolved observations, this results in a spectrum which is the sum of the spectra of each component. While this can often appear similar to the spectrum of a single greybody, especially for small temperature differences, fitting a single greybody spectrum results in a temperature which has limited physical meaning and is easily misinterpreted.

In light of the challenges application of fitting a single greybody to observation of box-wing satellites, we propose a two-component model where the spectrum is modelled as the sum of two independent greybody components. Mathematically this is expressed,

$$I(\lambda, A_C, \varepsilon_C, T_C, A_H, \varepsilon_H, T_H) = A_C \varepsilon_C B(\lambda, T_C) + A_H \varepsilon_H B(\lambda, T_H) \tag{5}$$

Where the first term gives the spectrum of the colder component, and the second term gives the spectrum of the warmer component. We remark that our aim is to infer the temperature of both the hot and cold components from spatially-unresolved observation of their combined thermal infrared spectrum. Therefore, our model represents a conceptual leap over previous approaches by distinguishing intra-RSO temperature differences. This is expected to allow better measurements of temperature changes across the RSO and thus operational monitoring. Techniques and understanding developed here to distinguishing intra-RSO temperatures may also serve as foundation building more detailed RSO spectral models.

Equation (5), is ill-suited to inference from observations; the parameters A_i and ε_i are degenerate, and large correlations in changes to the spectrum exist between the cold and hot component temperatures (T_C and T_H respectively). Rather, we choose to parameterize this model via, an effective area $\alpha = \varepsilon_C A_C + \varepsilon_H A_H$, the fraction the cold blackbody contributes to the effective area $f_C = \varepsilon_C A_C / \alpha$, an effective temperature of the spectrum $T_{\text{eff}} = f_C T_C + (1 - f_C) T_H$ indicative of the temperature fitting a single greybody to the RSO spectrum would achieve, and the difference between the hot and cold component temperatures $\Delta T = T_H - T_C$. Using this parametrization the two-component spectral model is expressed:

$$I(\lambda, \alpha, f_C, T_{\text{eff}}, \Delta T) = \alpha \Big(f_C B(\lambda, T_{\text{eff}} - (1 - f_C)\Delta T) + (1 - f_C) B(\lambda, T_{\text{eff}} + f_C \Delta T) \Big) \tag{6}$$

We visualize this spectrum and the contribution from both the hot and cold components for parameters of $\alpha = 1, f_C = 0.7, T_{\text{eff}} = 300\,\text{K}$ and $\Delta T = 70\,\text{K}$ in fig. 4. Of these four parameters to our model, ΔT is of particular interest for satellite monitoring. Unlike the other parameters of our model, ΔT has a direct physical interpretation of the difference between the hot and cold component temperatures. It is therefore independent of many other confounding RSO parameters such as attitude, range, or surface properties. Furthermore, it follows from eq. (2) that changes in power flow between RSO components will result in large changes to ΔT. For instance, spacecraft operations which draw power from the solar panels for activities in the chassis will result in a negative P_{int} for the solar panels and an equivalent positive P_{int} into the chassis. This results in a reduction of the steady state value of ΔT. The specific relationships between ΔT, power flow and individual component temperatures for the example solar array and spacecraft chassis considered in table 1 is shown in fig. 5. The maximum power flow shown in this figure represents a solar panel efficiency of 22 %. Over this range of power flows ΔT decreases by 66 K at a near-constant rate.

4. INFERENCE FROM INFRARED OBSERVATIONS

4.1 Methods

To explore the uncertainty to which RSO component temperatures can be inferred, we model our observations as measurements at the central wavelength of eight logarithmically spaced points between 3 µm to 10 µm each with an SNR of 1000. As demonstrated by the serendipitous observation of Echostar 4 by the WISE space telescope fig. 2, this is both a technologically feasible wavelength range and the observed SNR in this exposure imply that this SNR of 1000 is achievable for geostationary spacecraft with ≈ 5 min exposures from a ≈ 0.5 m diameter aperture space telescope.

Copyright © 2025 Advanced Maui Optical and Space Surveillance Technologies Conference (AMOS) – www.amostech.com

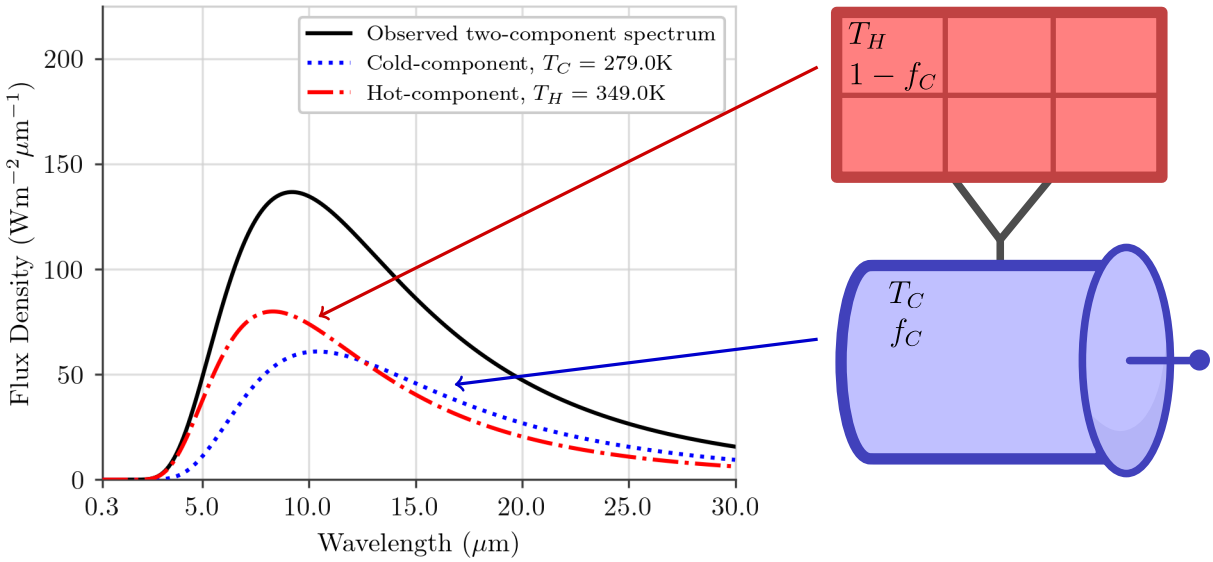

Fig. 4: A satellite's spectrum contains detailed information about each component. This information is lost when considering only a single characteristic temperature for the satellite. Modeling the temperature and spectral emissions of each component in a multi-component model can recover more information about a satellites activities and operations. We plot our proposed two-component spectrum (eq. (6)) (black) and the spectral contribution of the two greybody components (red and blue) representative of a satellite's chassis and solar arrays. Due to geometry and material properties, planar solar arrays are expected to attain a greater steady state temperature than the chassis. This difference further implies that a single greybody fit to the spectrum has only limited physical meaning.

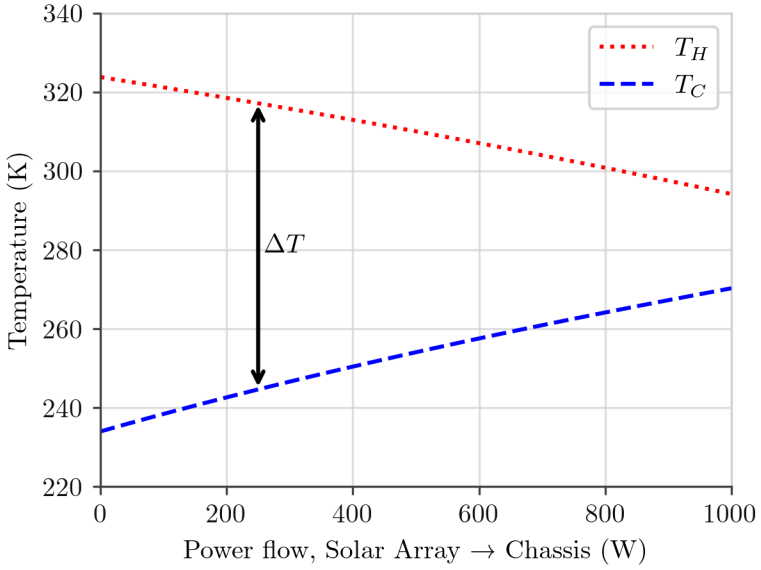

Fig. 5: Steady state temperatures for a example box-wing type satellite composed of the chassis and solar array components described in table 1. Power flows from the solar arrays to the chassis result cooler array temperatures and warmer chassis temperatures. The temperature difference between these two components, ΔT, is a strong indicator of power flow and therefore satellite activities.

Copyright © 2025 Advanced Maui Optical and Space Surveillance Technologies Conference (AMOS) – www.amostech.com

For a given observation, we fit our two-component model via a `scipy` implementation of the trust region reflective non-linear least-squares algorithm[1]. Parameter bounds of $\alpha \in (10^{-2}, 10^{2})$, $f_C \in [0,1]$, $T_{\text{eff}} \in [100\,\text{K}, 700\,\text{K}]$, and $\Delta T \in [0\,\text{K}, 600\,\text{K})$ are used during the fitting process. We find that robust curve fitting requires an analytic or automatic differentiated Jacobian of eq. (6) due to this Jacobian becoming singular in the limits $\Delta T \to 0$, $f_C \to 0$, and $f_C \to 1$. Furthermore, as in these limits, the spectrum converges to that of a single greybody, only one component is needed to describe the data. The other component is thus free to fit the residuals and does not provide physically meaningful information about the RSO. In these cases the non-physically meaningful component contributes only a small amount to the flux. To ensure the thermal model provides physically meaningful results on actual data, we must consider realistic bounds on the percentage of flux that is attributed to each component of the satellite. We therefore only consider fits where both components have sum of the flux in each wavelength greater than 1 % of the total flux to ensure both components provide physically meaningful information about the RSO.

Due to the inherent noise in observations, the fitted parameters ($\hat{\alpha}, \hat{f_C}, \hat{T_{\text{eff}}}$ and $\hat{\Delta T}$) returned by the least-squares regression will differ from the true parameters ($\alpha_0, f_{C0}, T_{\text{eff}0}$, and ΔT_0) by some random amount. To characterize this difference, and thus uncertainty in the fitted parameters, we calculate fit parameters for many realizations of the observation to build their sampling distribution. From the sampling distribution of each of the parameters we use the root mean square error (RMSE) as a measure of the uncertainty:

$$\sigma(\hat{\theta}) = \sqrt{\frac{1}{N}\sum_{i}^{N}\left(\hat{\theta}_i - \theta_0\right)^2}, \tag{7}$$

where θ is a parameter, $\hat{\theta}_i$ the fit of parameter θ obtained from realization i, and N the total number of realizations.

4.2 Results

Overall, our results show that the two component thermal model proposed in this work accurately describes and measures component temperature of a box-wing type satellite. First, fig. 6 displays how the parameter uncertainties change with varying ΔT_0 and at $\alpha_0 = 1$, $f_{C0} = 0.7$, and $T_{\text{eff}0} = 300\,\text{K}$. Inference is possible for all parameters over a wide range of ΔT_0 values with the greatest uncertainties observed in $\hat{f_C}$ and $\hat{\Delta T}$. These parameters also exhibit large increases to uncertainty at decreasing ΔT_0. This is expected due to these parameters resolving the two greybody components, the difference between which vanishes in the limit of $\Delta T_0 \to 0$. $\hat{\alpha}$ and $\hat{T_{\text{eff}}}$ exhibit little dependence on ΔT_0. Above a ΔT of 30 K all parameters can be resolved to within 15 %. In particular, at $\Delta T_0 > 30\,\text{K}$, $\hat{\Delta T}$ has uncertainty less than 2.1 K, and $\hat{T_C}$ and $\hat{T_H}$ can both have uncertainties of less than 4.2 K and 4.6 K respectively. ΔT_0 above 30 K is expected for typical box-wing type satellites and hence our results show that these component temperatures are able to be inferred to within a few Kelvin. In particular we note that, using the model provided in eq. (2) and example components from table 1, these uncertainties allow for satellite power flows to be monitored to within 50 W at a $\hat{\Delta T}_0 = 30\,\text{K}$.

In infrared telescopes, the astrophysical sky background contributes to the background noise and thermal emission from the telescope baffle contributes to the foreground noise of any observation [18]. This is especially problematic at longer observation wavelengths and at warmer baffle temperatures. While the astrophysical sky background is constant, the design of infrared space telescopes require significant thermal engineering to maintain sufficiently cool baffle temperatures and the resultant cost and complexity of the design increases with the cooler temperatures required to observe at longer wavelengths. It is therefore important to understand the maximum observation wavelength required for inference of our two-component model.

To evaluate the benefit longer wavelengths provide for parameter uncertainty and thus their necessity for an infrared space telescope for space domain awareness, fig. 7 presents the dependence on inferred parameter uncertainty on maximum observation wavelengths. Results were obtained using the method outlined in section 4.1 with eight logarithmically spaced bands however with a varying maximum wavelength for this spacing. While the maximum achievable SNR in each wavelength is variable, in this study we use a conservative constant SNR value achievable in all bands to keep our findings relevant beyond the specifics of any particular infrared space telescope. Parameter uncertainty is seen to decrease with an increase in observation wavelength range. With respect to maximum wavelength, parameter inference uncertainty for all parameters of our model is seen to greatly increase at maximum wavelengths below 10 µm. At wavelength above 15 µm parameter uncertainties in $\hat{f_C}$, $\hat{\Delta T}$, $\hat{T_C}$, and $\hat{T_H}$ are seen to plateau. This suggest that

[1] https://docs.scipy.org/doc/scipy/reference/generated/scipy.optimize.curve_fit.html

Copyright © 2025 Advanced Maui Optical and Space Surveillance Technologies Conference (AMOS) – www.amostech.com

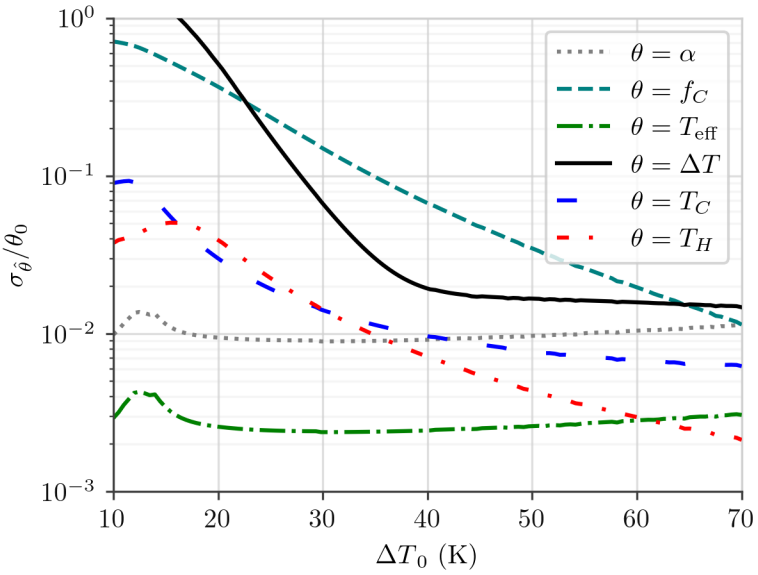

Fig. 6: Parameter uncertainties of inference of the parameters of our two-component model (eq. (6)) from observation at $\alpha_0 = 1$, $f_{C0} = 0.7$, $T_{\text{eff}0} = 300\,\text{K}$ and varying ΔT_0 (temperature difference between the satellite's hot and cold components). Given ΔT_0 much greater than 10 K is expected, inference of our model is thus possible over a wide range of the feasible parameter space. These uncertainties describe how well satellite component temperatures, such as those of the chassis and solar arrays can be inferred from unresolved observations by an infrared space telescope.

wavelengths above 15 µm are not important resolving multiple greybody components from the spectrum. Likewise, only small decreases in the parameter uncertainties of $\hat{\alpha}$ and $\hat{T_{\text{eff}}}$ occur beyond this point. Given the design challenges of observations at longer wavelengths, it is likely that these results imply infrared space telescopes for satellite monitoring should prioritize higher SNR - either via a larger aperture or longer observation time - over measurement at wavelengths longer than 10 µm. Possibly there would be value in considering a cut-off at $\sim 10 - 12$µm, depending on cost differential with a 15 µm cut-off. We, however, leave estimating the specific additional cost and technical complexity of specific wavelength cut-offs to future work.

At shorter wavelengths solar radiation begins to dominate the RSO spectrum. This either makes neglecting solar radiation a poor assumption, restricts observation conditions, or requires more sophisticated techniques to subtract this solar spectrum. The significant temperature dependence of the infrared flux at shorter wavelengths suggest measurement and greater spectral resolution at these shorter wavelengths is beneficial to temperature inference. Without subtracting the solar spectrum this is possible down to a minimum wavelength of approximately 3 µm.

Electric thrusters on spacecraft can reach temperatures of several hundred Kelvin above the chassis temperature when used for maneuvering, thus, their greybody emissions would peak at about 4 µm. While not part of our two-component model presented here, an extension to our model could also infer the presence of emission from an electric thruster in the observed spectrum and thus monitor spacecraft maneuvering. Shorter wavelength observations would also aid this maneuver detection capability.

5. CONCLUSION

In this paper, we outline the principles behind monitoring satellites from spatially unresolved infrared observations noting how the infrared emission spectrum holds rich information about spacecraft operations and activities and thus offer unique monitoring opportunities to compliment radar and optical observations. We highlight the limitations of fitting a single greybody spectrum of box-wing type satellites and thus propose a two-component spectral model which better describes the different temperature and power dependence of the chassis and solar arrays. From our model we note that the temperature difference between the two-components ΔT serves as a key indicator for spacecraft activities. We forecast that the parameters of our two-component model can be reliably estimated from unresolved thermal infrared

Copyright © 2025 Advanced Maui Optical and Space Surveillance Technologies Conference (AMOS) – www.amostech.com

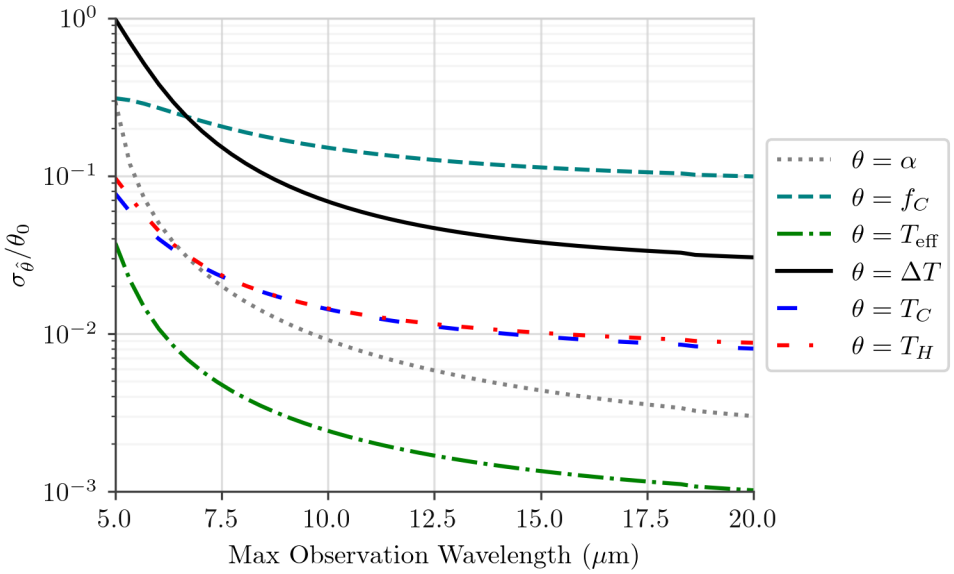

Fig. 7: Parameter inference uncertainties for our two-component model (eq. (6)) from observation in eight logarithmically spaced bands at varying maximum observation wavelength and fixed minimum of 3 µm. True parameters of $\alpha_0 = 1$, $f_{C0} = 0.7$, $T_{\text{eff}0} = 300\,\text{K}$, and $\Delta T_0 = 30\,\text{K}$ are used. Observation at longer wavelengths are technically more challenging in part due to the baffle cooling needed to limit foreground emissions. Observing at above 15 µm provides only limited benefit to inference uncertainties.

observations by a $\approx 0.5\,\text{m}$ diameter aperture telescope and calculate the associated uncertainties to which parameters can be estimated. We find that above a ΔT of 30 K, well below what is expected in typical operation, spacecraft component temperatures can be inferred to within 5 K. Furthermore our results imply that for an example meter-sized satellite, power-flows from the solar arrays to the spacecraft chassis can be inferred to an uncertainty of 50 W. Finally, sensitivity of inference of our model was studied against maximum observation wavelength. Little benefit was found in observations longer than 15 µm. Future work should study simultaneous measurement in additional bands in the optical and near IR to subtract reflected sunlight and spacecraft maneuver detection via the short-wavelength spectral emissions of operating electric thrusters.

ACKNOWLEDGMENTS

This research is supported by the Australian Office of National Intelligence through the National Intelligence and Security Discovery Research Grant award NI230100162. This research is supported by an Australian Government Research Training Program (RTP) Scholarship. This research is partially based on information from ESA DISCOS (Database and Information System Characterising Objects in Space), a single-source reference for launch information, object registration details, launch vehicle descriptions, as well as spacecraft information for all trackable, unclassified objects. We acknowledge ESA's efforts to maintain and operate this database with its APIs.

6. REFERENCES

[1] Mark R Ackermann, Colonel Rex R Kiziah, Peter C Zimmer, J T McGraw, John T McGraw, J T McGraw, and David D Cox. A SYSTEMATIC EXAMINATION OF GROUND-BASED AND SPACE-BASED APPROACHES TO OPTICAL DETECTION AND TRACKING OF SATELLITES. In *31st Space Symposium*, April 2015.

[2] James Allworth, Stuart Bartlett, Samantha Kirkwood, Karla Vincent, Hannah Dawe, Jack Sines, Toby Harris, Hiranya Jayakody, and William Crowe. The Use of Flyby Space-to-Space Non-Earth Imagery to Rapidly Identify and Characterise Unknown Objects. In *Advanced Maui Optical and Space Surveillance Technologies Conference*, Maui, Hawai'i, 2024.

Copyright © 2025 Advanced Maui Optical and Space Surveillance Technologies Conference (AMOS) – www.amostech.com

[3] Jianli Du, Junyu Chen, Bin Li, and Jizhang Sang. Tentative design of SBSS constellations for LEO debris catalog maintenance. *Acta Astronautica*, 155:379–388, February 2019.

[4] Joshua Fitzmaurice. *STREAK DETECTION AND PHOTOMETRY WITH THE NASA WIDE-FIELD INFRARED SURVEY EXPLORER*. M.Sc, Royal Military College of Canada, May 2018.

[5] E. M. Gaposchkin and R. J. Bergemann. Infrared Detections of Satellites with IRAS:. Technical report, Defense Technical Information Center, Fort Belvoir, VA, September 1995.

[6] E.M. Gaposchkin, C. Von Braun, and J. Sharma. Space-based space surveillance with the Space-Based Visible. *Journal of Guidance, Control, and Dynamics*, 23(1):148–152, 2000.

[7] John Kielkopf and Frank O Clark. Remote Sensing of Satellite Activity through Optical and Infrared Temporal Differential Spectrophotometry Informed by Analysis of Noise. In *Advanced Maui Optical and Space Surveillance Technologies Conference*, Maui, Hawai'i, 2022.

[8] Robert Leitch and Ian Hemphill. Sapphire: A Small Satellite System for the Surveillance of Space. In *24th Annual AIAA/USU Conference on Small Satellites*, 2010.

[9] James G. (Gil) Miller. A New Sensor Allocation Algorithm for the Space Surveillance Network. *Military Operations Research*, 12(1):57–70, 2007.

[10] Daniel O'Connell, Jean-Claude Leclerc, Noemi Giammichele, Ryan Comeau, Narendra Gollu, Naron Phou, and Frederic Pelletier. Concept of Operation and Initial Performance Summary of the NorthStar Space-Based Optical SSA System. In *Advanced Maui Optical and Space Surveillance Technologies Conference*, Maui, Hawai'i, 2024.

[11] Corey D Packard, Casey D Demars, Logan R Canull, David W Tyler, Christopher Rodgers, Zachary J. Edel, and Timofey Golubev. Dynamic EO/IR Satellite Signature Predictions with High-Fidelity MuSES Simulation. In *Dynamic EO/IR Satellite Signature Prediction with High-Fidelity MuSES Simulation*, Maui, Hawai'i, 2024.

[12] Charles Paxson, Hilary E. Snell, James M. Griffin, Kathleen Kraemer, Steve Price, Mike Kendra, and Don Mizuno. Space Object Temperature Determination from Multi-Band Infrared Measurements:. Technical report, Defense Technical Information Center, Fort Belvoir, VA, September 2008.

[13] Eric C. Pearce, Harrison Krantz, Adam Block, and Deatrick L. Foster. Infrared photometry and spectrometry of satellites and debris at UKIRT. *Journal of Space Safety Engineering*, 11(3):432–438, September 2024.

[14] Jacqueline A. Reyes, Heather M. Cowardin, and Miguel Velez-Reyes. Analysis of Spacecraft Materials Discrimination Using Color Indices for Remote Sensing for Space Situational Awareness. *The Journal of the Astronautical Sciences*, 70(5):33, September 2023.

[15] Timothy Sejba. Space Domain Awareness: Doctrine for Space Forces, November 2023.

[16] Hanqing Sun and Yuantian Qin. Stealthy Configuration Optimization Design and RCS Characteristics Study of Microsatellite. *Aerospace*, 9(12):815, December 2022.

[17] J. Utzmann, A. Wagner, Jiri Silha, Thomas Schildknecht, P. Willemsen, F. Teston, and T. Flohrer. Space-based space surveillance and tracking demonstrator: mission and system design. In *Utzmann, J.; Wagner, A.; Silha, Jiri; Schildknecht, Thomas; Willemsen, P.; Teston, F.; Flohrer, T. (2014). Space-based space surveillance and tracking demonstrator: mission and system design. In: Proceedings of 65th International Astronautical Congress (pp. 1648-1655). International Astronautical Federation (IAF)*, pages 1648–1655, Toronto, Canada, 2014. International Astronautical Federation (IAF). Num Pages: 7.

[18] Raymond H Wright, Michael Gordon, Jeffery E Van Cleve, and Hans Schroots. Infrared Sensing for Space-Based Space Domain Awareness. In *Advanced Maui Optical and Space Surveillance Technologies Conference*, Maui, Hawai'i, 2023.

Copyright © 2025 Advanced Maui Optical and Space Surveillance Technologies Conference (AMOS) – www.amostech.com